Unmoderated Molten Salt Reactors design optimisation for power stability

A. Laureau[a,b], A. Bellè[c,d], M. Allibert[b], D. Heuer[b], E. Merle[b], A. Pautz[c,e]

[a]*SUBATECH, CNRS/IN2P3, IMT-Atlantique, F-44307 Nantes, France*
[b]*LPSC, Université Grenoble-Alpes, CNRS/IN2P3, 53 rue des Martyrs, F-38026 Grenoble Cedex, France*
[c]*LRS, Ecole Polytechnique Fédérale de Lausanne (EPFL), CH-1015 Lausanne, Switzerland*
[d]*Chair on Risk and Resilience of Complex Systems, Laboratoire Génie Industriel, CentraleSupélec, Université Paris-Saclay, France*
[e]*Nuclear Energy and Safety Research Division (NES), Paul Scherrer Institut (PSI), CH-5232 Villigen, Switzerland*

Abstract

The critical region of unmoderated molten salt reactors consists in a cavity filled with a liquid fuel. The lack of internal structure implies a complex flow structure of the circulating fuel salt. A preliminary core shape optimization has been performed during the EVOL European project to limit recirculation and hotspots. This optimization was based on a Reynolds Averaged Navier Stokes (RANS) approach, but the latter only provides time-averaged values for velocity and temperature. However, the power stability is sensitive to thermal fluctuations induced by the flow turbulence itself, even at steady state without pump flow rate or heat extraction variation. This phenomenon is studied using a Detached Eddies Simulation approach to solve the turbulence in the reactor and get a time dependent temperature distribution and then the reactivity fluctuations. A new geometry is proposed to limit the total power fluctuations from 7.5 % for the preconceptual EVOL geometry down to 1.2 %.

Keywords: DES, Turbulence, Reactivity fluctuation, Core design, Molten salt reactor

1. Introduction

Unmoderated Molten Salt reactors with a liquid circulating fuel have in common a tank-like structure allowing a free flow distribution in the critical region of the fuel circuit. For this reason, Computational Fluid Dynamics (CFD) codes are typically used for velocity and temperature distribution calculations [1, 2, 3, 4]. CFD calculations are often performed using Reynolds Averaged Navier Stokes (RANS) approaches due to the computational cost of CFD codes. This approach consists to model the turbulence using different turbulence models such as the k-ϵ realizable one where k is the turbulent kinetic energy and ϵ the associated dissipation rate. Thanks to this modeling, the effect of the turbulence is correctly taken into account on the average flow distribution.

Figure 1 illustrates the kind of results that a RANS approach can provide for the Molten Salt Fast Reactor (MSFR) [6] study using the "EVOL" geometry (developed in the frame of the European project EVOL [7]). The velocity and temperature distributions are smooth in the core, with a uniform rise of the temperature.

However, even if the influence of the turbulence is correctly taken into account for the average distribution, the turbulence is modeled and not numerically solved. A local temperature fluctuation due to turbulence would impact the reactivity and then produce a power fluctuation. Characterizing these power fluctuations is important to further optimize the design, and then the eddies have to be numerically solved with more complex tools. For this reason, a refined modeling based on Large Eddies Simulation (LES) has been used in this article to study how the local thermal fluctuations interact with neutronics through the density and Doppler feedback effects. Note that LES calculation has been used in previous studies on specific components of the thorium molten salt reactor such as a gas-liquid separator [8] but not at the core scale.

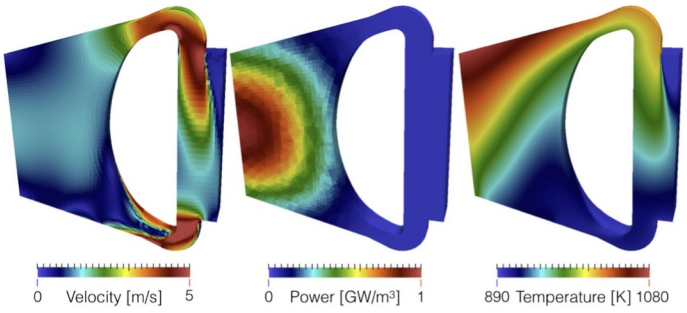

Figure 1: $1/32^{nd}$ MSFR system with the core center (critical region) on the left of the geometry and the heat exchanger on the right. The different distributions are the velocity (left), the power(middle) and the temperature (right) [5].

Preliminary technical elements needed for this kind of calculations are explained in section 2 concerning neutronics (reactivity variation estimation) and thermal hydraulics (meshing requirements). Then the results obtained on the EVOL geometry are discussed in section 3 together with a new optimized design taking into account

these new developments and presented in this paper. Finally a quantitative comparison of the reactivity fluctuations for both cases is also discussed.

2. Physics introduction

2.1. Neutronics

In order to optimize the core to minimize reactivity fluctuations, an estimation of the reactivity according to a given temperature map is necessary. A precise neutronic calculation such as direct Serpent2 [9] calculation using a temperature snapshot requires a large calculation time, especially to limit the statistical fluctuations and thus to refine correctly the fluctuations within a few pcm. For this reason, a simplified reactivity estimation based on local feedback effects is used. Section 2.1.1 presents the interpolation of the Doppler and of the density feedback with temperature, and section 2.1.2 presents a spatial weighting to take into account the location of the temperature variations. We consider here the reference MSFR system [10, 6] (*i.e.* a breeder reactor operated in the Th/^{233}U fuel cycle and with a fluoride salt) as a starting point for the calculations. Similar results can be obtained for other salt compositions and fuel cycles. For this reason and to be more generic, we focus on the effective temperature variation rather than on the reactivity variation. In this way, for another feedback coefficient, the reactivity variation can be obtained.

2.1.1. Doppler and density feedback effects

Doppler and density feedback effects originate from different physical phenomena and have different temperature dependences. The Doppler effect is due to neutron cross section broadening when the nucleus agitation increases with temperature. This effect increases the capture rate for reactors with fertile elements in the fuel. The density feedback in an unmoderated liquid fuel reactor is equivalent to increase the leakage rate (neutron mean free path increase).

The temperature dependence for a variation on the whole reactor is presented in figure 2, the points correspond to the Monte Carlo estimation with the corresponding statistical uncertainties. Each Serpent2 calculation corresponds to a point in the top plot (which represents ρ as a function of the temperature), and they are combined for a variation of 100 K to estimate the local reactivity derivative (bottom). The Doppler dependency is logarithmic, and the density follows a second order polynomial trend. The plain lines are the results of the fitted curves using the 800 K-1800 K region, the points from 300 K to 700 K are here for illustration purpose and to confirm the Doppler trend.

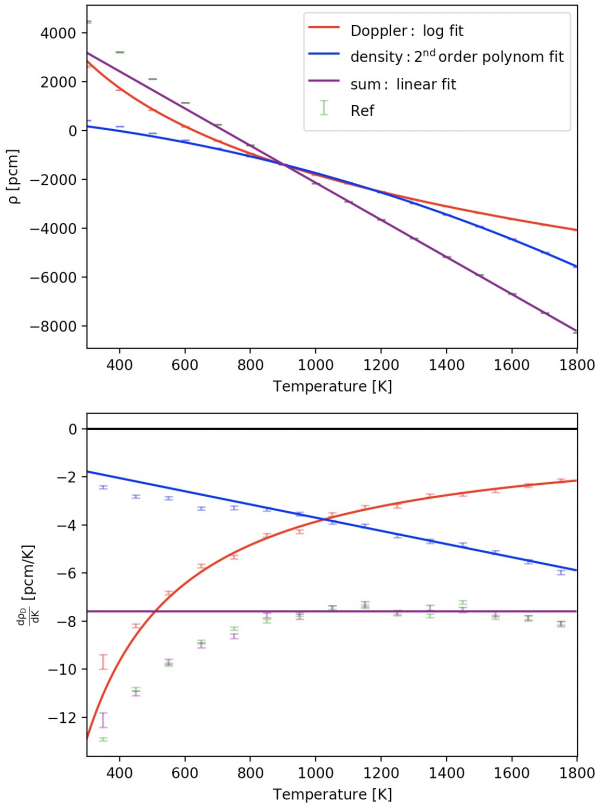

Figure 2: Reactivity feedback due to Doppler (red) and density (blue) feedback, the sum of the components (purple), and a reference calculation with both effects in green. The top curve displays the reactivity as a function of temperature, and the bottom one the reactivity derivative with temperature.

Considering both Doppler and density feedback effects, we can see that the local non-linearities are compensating and then, in the 900 K-1500 K range, the total feedback coefficient can be considered as constant. Note that this value is reasonable for the MSFR classical 3 GW Th-U cycle but can be different for another reactor with a different Doppler/density response.

2.1.2. Feedback distribution

The second aspect to consider is the feedback distribution in the core. For example, the impact in the core center is larger than in the periphery. The expected distribution for a local absorption modification is a distribution close to the neutron flux distribution multiplied by the adjoint flux. The flux weighting is due to the proportionality between the probability that a neutron "sees" the absorption perturbation and the amplitude of the reactivity response. The adjoint flux weighting corresponds to the importance that the induced perturbation has on the chain reaction. In a first approximation, the adjoint flux being close to the neutron flux in a homogeneous reactor, we can test the Doppler feedback on a squared flux distribution provided by the Monte Carlo neutron transport code Serpent2. Concerning the density feedback, this reasoning (adjoint flux multiplied by the neutron flux) is not

valid since it does not locally change the absorption rate but it increases the mean free path and then the neutron loss.

Two cases are compared:

- The first case (figure 3) presents the density and Doppler feedback distributions for a 2 meter cubic reactor with reflection on the X/Y boundaries and with leakage on the Z boundary.
- The second case (figure 4) is a 2 meter cubic reactor with a 20 cm thick Hastelloy-N reflector and neutron loss boundary conditions.

For both cases, a local axial perturbation of +300 K is applied, modifying the temperature (Doppler) and the density separately.

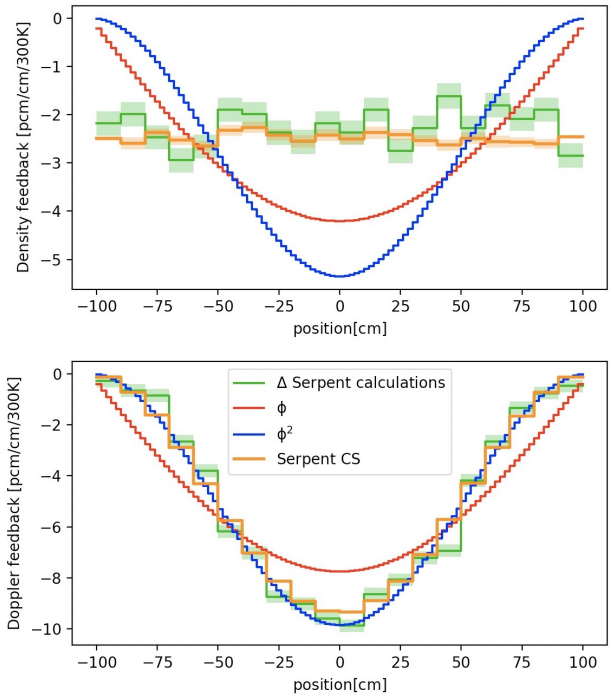

Figure 3: Density (top) and Doppler (bottom) feedback distributions for a uniform 1D-axial perturbation in a cube reactor with radial reflection and axial leakage boundary conditions. The bottom of the reactor corresponds to -100 cm on the abscissa and the top to +100 cm.

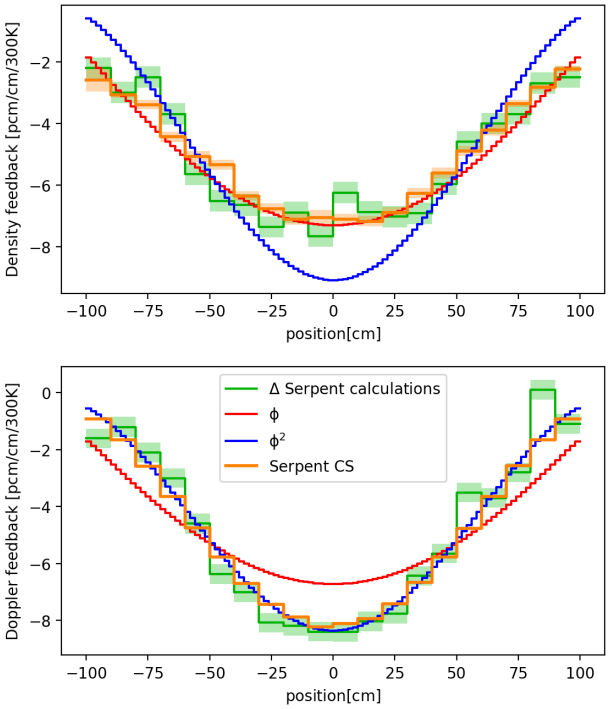

Figure 4: Density (top) and Doppler (bottom) feedback distributions for a uniform 1D-axial perturbation in a cube reactor surrounded by a reflector and with leakage boundary conditions. The bottom of the reactor corresponds to -100 cm on the abscissa and the top to +100 cm.

Different curves are presented, the green results come from direct Monte Carlo calculations (initial temperature distribution reactivity difference with a local perturbation of 300K). This result is compared to the orange curve which is the result of a Monte Carlo calculation with a Correlated Sampling (CS) implementation for local feedback estimation [11]. A lower statistical noise is expected with this method since the two systems (analog and modified) are studied using the same neutron tracks, modifying the neutron weight accordingly. Finally, the red and the blue curves correspond to the neutron flux and the squared neutron flux distribution in the system. These two distributions are normalized to the global feedback amplitude so that, if the Doppler feedback matches with a squared flux distribution, the curves should be the same.

We can see in figure 3 that the density feedback distribution is flat for a homogeneous system with radial reflective boundary conditions. This is an interesting result since it highlights that the density feedback distribution is not supposed to follow a squared flux distribution. A perfectly constant distribution is expected because of the radial reflective boundary condition: only the total amount of fuel between the top and the bottom determines the reactivity. Regarding the Doppler effect, we can see that both the Monte Carlo and the CS results are estimating a feedback distribution very close to the squared flux distribution.

Considering the more realistic case (figure 4) with a neutron reflector plus a radial leakage boundary condition,

we can see that the conclusions are very similar for the Doppler effect, and a distribution based on the squared neutron flux is a very good approximation.

Regarding the density feedback reaction, the distribution is very close to the flux distribution. This can be linked to the radial neutron leakage that is larger at the core center rather than in the top and bottom positions. However this result should be dependent on the reactor geometry and composition. For this study, only an estimation of the feedback distribution is required to evaluate and compare multiple core designs but, for a transient calculation or a safety study, a more precise approach is recommended.

Finally, the reactivity feedback estimation is performed in two steps. For a given core design, the Serpent2 code is used to estimate the power distribution in the core using the thermal hydraulics mesh thanks to the Serpent2 CFD mesh reading capabilities. Then, in the OpenFOAM calculation at each time step, the temperature field is weighted by the power field and the squared power field. Finally, these two temperatures are equally combined to provide an effective temperature (Doppler and density feedback amplitudes are equivalent at the nominal temperature).

2.2. Thermal Hydraulics

The usual CFD approach is split into 3 different families: RANS approaches (presented in figure 1), Large Eddy Simulation (LES) approach and Direct Numerical Simulation (DNS) approach [12]. The LES approach solves the larger scales of the turbulence and uses numerical models to take into account the effect of the isotropic eddies with a size smaller than the meshes. The DNS solves all the turbulence scales from the macroscopic one down to the viscous fluid relaxation.

Due to the numerical complexity, DNS calculations cannot be performed on this kind of case (3D complex geometry and a Reynolds number of around 10^6). A full LES calculation requires strong constraints on the meshes close to the walls to maintain a y-plus (dimensionless wall distance) close to one and to avoid a large aspect ratio in the meanwhile [13]. For this reason, hybrid approaches (Detached Eddy Simulation – DES) have been developed to combine LES resolution in the main flow region with RANS resolution close to the wall in order to use wall functions and to reach a y-plus between 30 to 300 (wall function validity domain).

For this reason, a DES approach is used here with the OpenFOAM CFD code [14] in order to simplify the wall resolution with a correct eddy resolution in the core and a correct reactivity fluctuation estimation. Two quantities have to be estimated in order to produce a valid DES mesh: the y-plus for the boundary layer and the mesh size in the core.

2.2.1. Y-plus estimation

The dimensionless wall distance characterizes the flow regime close to the wall: the viscous sublayer ($y^+ < 5$), the buffer layer ($5 < y^+ < 30$) and the log layer ($30 < y^+ < 300$). The expected y-plus for a given flow velocity U and a characteristic length L using the following equations based on a correlation on the skin friction C_f (valid if $Re < 10^9$), the wall shear stress τ_ω and the friction velocity u_*:

$$Re = \frac{\rho U L}{\mu} \tag{1}$$

$$C_f = \left(2\log_{10}(Re) - 0.65\right)^{-2.3} \tag{2}$$

$$\tau_\omega = C_f \frac{1}{2}\rho U^2 \tag{3}$$

$$u_* = \sqrt{\frac{\tau_\omega}{\rho}} \tag{4}$$

$$y = \frac{y^+ \mu}{\rho u_*} \tag{5}$$

The wall distance corresponding to $y^+ = 1$ for different flow characteristics is presented in table 1. We can see that a value of around 0.025 mm is a good order of magnitude, thus for a high Reynolds wall function ($30 < y^+ < 300$) this provides a constraint on the mesh size at the wall of 0.75 mm and 7.5 mm. Note that this is an order of magnitude, this quantity can be post-processed by the CFD code to adapt the mesh.

U [m/s]	L [m]	y [mm] for $y^+ = 1$
2	2	3.0×10^{-2}
3	2	2.0×10^{-2}
2	0.3	2.4×10^{-2}
2	0.03	1.9×10^{-2}

Table 1: Expected y-plus values for different flow characteristics

2.3. Mesh size

The mesh size in the core is an important parameter since all the eddies with a size too small compared to the mesh size cannot be resolved and are modeled. An estimation of the mesh size requirement can be performed thanks to a classic RANS calculation. The turbulence length scale is given by equation 6 [15, 13].

$$l_0 \sim \frac{k^{3/2}}{\epsilon} \tag{6}$$

According to [13], a mesh size equal to $\frac{l_0}{5}$ should allow to solve 80% of the turbulent kinetic energy. The number of meshes varies from 5 to 15 depending on the source. For this reason we considered a value of 10 as a starting point and order of magnitude. The LES mesh size estimated according to the $k - \epsilon$ RANS calculation is displayed in figure 5. This provides a minimal characteristic size of 1.5 cm in the inlet region, and locally a lower value very close to the wall but this region is in the RANS region of the DES approach. It remains important to check that the results (velocity and temperature) are stable if we change the mesh size, even if a LES calculation is supposed to slowly converge to the DNS results.

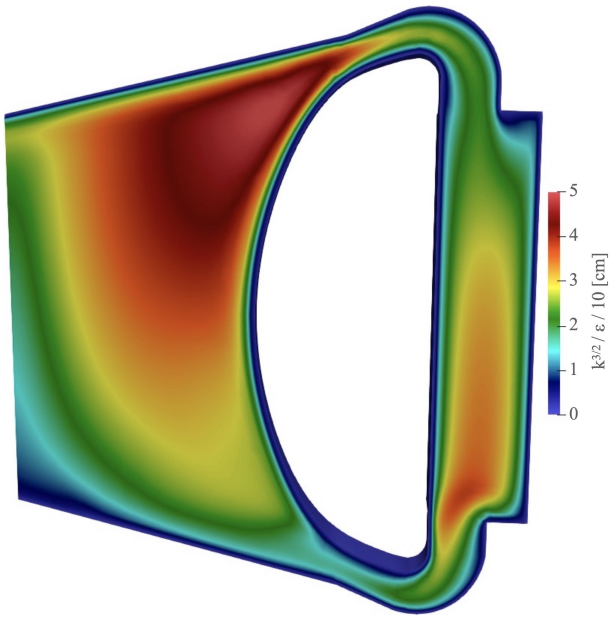

Figure 5: Mesh size in cm to respect a $l_0/10$ condition.

2.4. CFD modeling

The turbulence model used is the *k-omega-SST-DES* [16] implemented in OpenFOAM [14]. This model is based on an improved wall modeling capability of the Delayed Detached Eddy Simulation (*IDDES*) associated to a k-ω SST RANS modeling close to the wall. The thermophysical properties used are described in table 2. Note that the OpenFOAM code uses polynomial dependencies and the kinematic viscosity ν correlation is converted in a 4^{th} order polynomial fit.

	Formula	Unit	Range [K]
ρ	4094-0.882*(T-1008)	kg/m^3	[893, 1123]
ν	5.54e-8*exp(3689/T)	m^2/s	[898, 1119]
k_{th}	0.928+8.397 10^{-5}*T	$W/m/K$	[891, 1020]
C_p	-1111+2.78*T	$J/kg/K$	[867, 907]

Table 2: Thermophysical salt properties from MARS and ISTC projects [17, 18] for a LiF(78 %at.)-ThF_4(22 %at.) salt

The geometry is simplified here in the heat exchanger compared to the detailed geometry resulting from the EVOL European project [7], for an easier mesh generation and a better convergence. Moreover, the temperature and velocity are imposed in this region in order to limit the number of physical seconds simulated to reach the steady state. The temperature is imposed at 900 K and the velocity is adjusted to obtain a core flow rate of 4.5 m^3/s to correspond to the previous EVOL studies. These heat exchanger and pump simplifications cannot be used for a safety study (*e.g.* loss of heat sink), but this allows a more efficient optimization process for the core region.

The power shape is computed using the Serpent2 code using the reading and result export tools available with an OpenFOAM mesh. The total power is imposed to 3 GW and is kept constant with time. This simplification allows a faster convergence of the temperature profile to focus on the temperature fluctuations induced by turbulence.

3. Results obtained

3.1. EVOL geometry study

Two different meshes are presented here with 28.7 million meshes (fine) and 12.2 million meshes (coarse) to match the previous recommendations. Please note that, even if this mesh is referred as coarse, it is checking the mesh size recommendation for the DES resolution. Figure 6 presents the y-plus distribution in the fuel circuit for both meshes. Regarding the y-plus order of magnitude, both meshes are in the target range, and as expected the size of the first mesh impacts the y-plus value. We can see that the eddies impact on the wall has a smaller characteristic size.

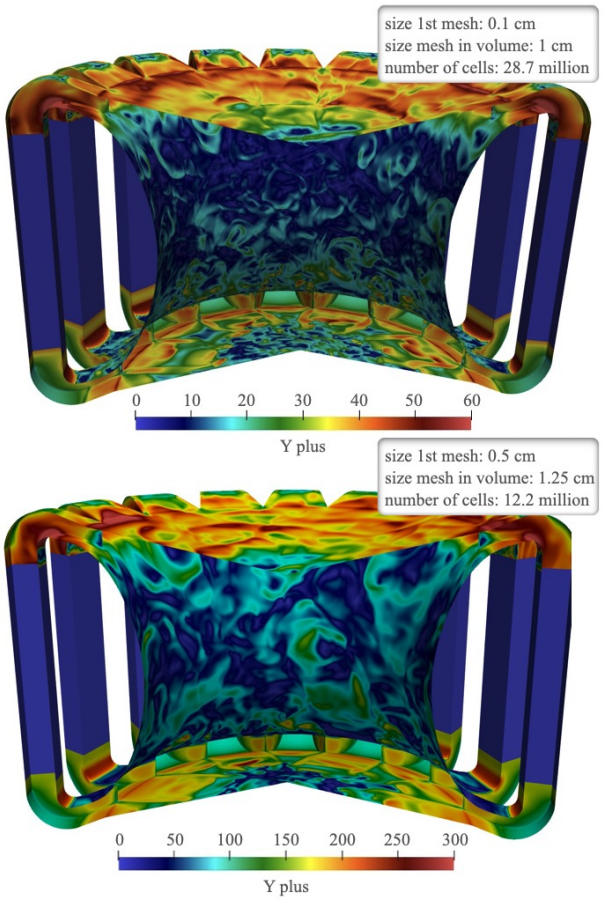

Figure 6: Y-plus distribution for two different simulated meshes: fine mesh (top) and coarse mesh (bottom).

Figure 7 presents the temperature and velocity distributions for the two meshes. We can see that the mesh quality impacts the size of the smaller eddies but not the overall distribution. This confirms that the mesh size seems correct and, as detailed in section 3.3, the reactivity fluctuations due to temperature fluctuations are very close between the two calculations. Compared to a classic

RANS calculation such as presented in figure 1, the flow distribution is more important in the core center and the recirculation size is more important along the main cavity walls with higher temperature. As we can see between different time steps, the recirculation size is not stable due to the turbulence, which implies reactivity fluctuations.

For these reasons, the core shape has to be optimized according to the DES calculation. Note that the DES calculation is expected to provide better results than the RANS calculation for this complex 3D configuration. However, the final result cannot be considered as perfect with CFD tools on a first of a kind system, only an experiment with a similar flow distribution should confirm the geometry.

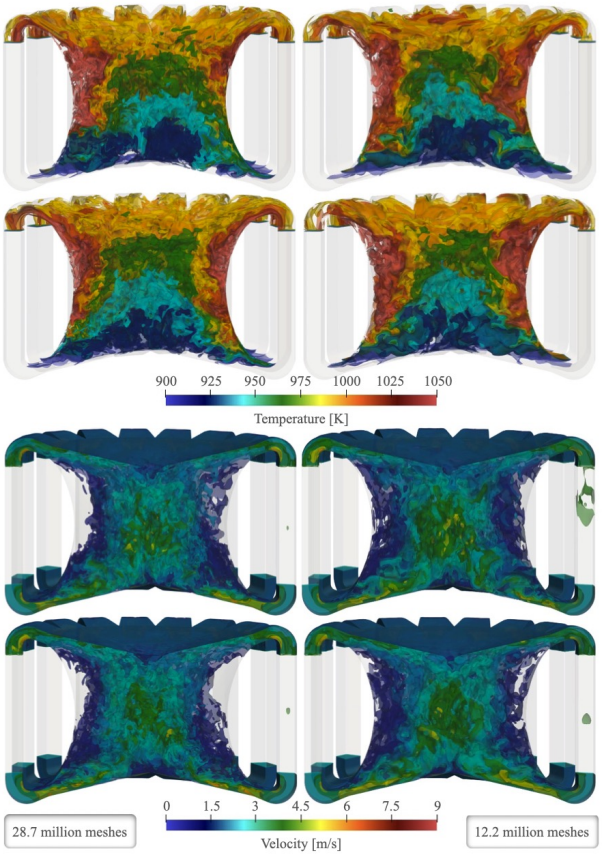

Figure 7: Temperature (top) and velocity (bottom) isovalues for the fine (left) and coarse (right) meshes at different time steps with the EVOL design.

3.2. Optimized geometry study

The EVOL geometry is a useful starting point, but it appears that this geometry initially based on RANS calculations has to be further optimized. Because of the large fluid inlet in the main cavity, the eddies in the core are large. These macroscopic eddies imply temperature and then reactivity fluctuations. For this reason, a structure breaking the flow in multiple sub inlets should help to reduce these fluctuations. Moreover the core shape and injection have to be modified to avoid a large recirculation zone close to the wall leading to large temperatures.

The main cavity radius is 1.12 m and the height is 2 m. As for the EVOL geometry, this design is composed of independent sectors (*i.e.* recirculation loops) composed of one pump, one heat exchanger and the pipes. Many different configurations have been tested up to the proposed design in figure 8 with 8 different sectors (instead of 16 for the EVOL geometry). These sectors are settled in the reactor vessel with a radius larger than the heat exchanger position, and the critical zone that corresponds to the main cavity in the CFD calculations is the free space left between the different sectors.

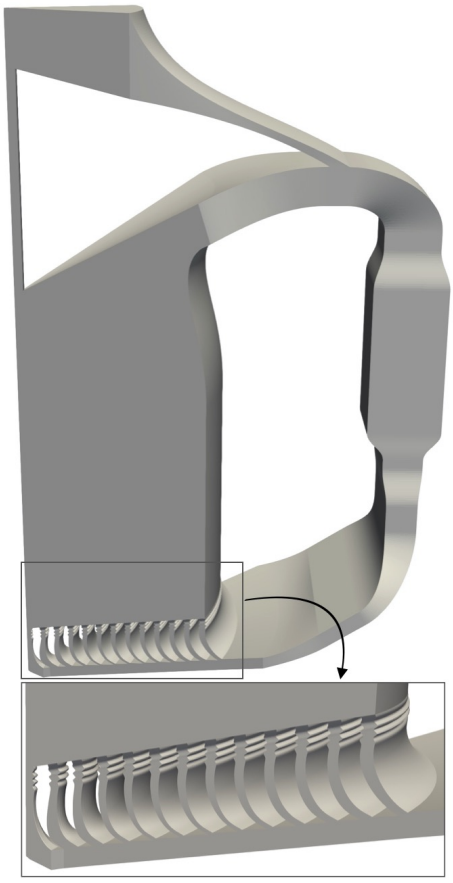

Figure 8: Optimized geometry ($1/8^{th}$) visualization using paraview [19].

Some observations can be already noticed. First a core injection with multiple blades allows to decrease the eddies size, and the blade curvature helps the fluid to go from the inlet pipe to the core cavity. These blades can be welded together with two plates going from the center up to the wall as visible at the bottom of figure 8 with the shift between the cavity surface and the blades. Then the injection pieces for the whole core would consist of 8 triangles composed of 12 blades. The space between the blades is adjusted to optimize the flow distribution, a uniform flow in the core center helps to limit the reactivity fluctuations while a uniform flow distribution close to the wall limits the temperature on the materials. Thus, it is

possible to assume that these blades can be replaced in order to adjust the flow distribution in the core if needed. Finally, in order to optimize natural convection in future studies, the heat exchanger region is settled at a higher position than the critical region. Note that the volume in the critical area is similar to the EVOL geometry (around $8\,m^3$) even if this volume cannot be perfectly defined with the complex 3D outlet shape.

The temperature and velocity distributions are presented in figure 9 for the fine (25.6 million) and coarse (15.1 million) meshes. We can see that the temperature is rising smoothly in the core without recirculation close to the wall. A recirculation with a ring shape still exists for intermediate radius at the bottom of the core with a higher temperature close to the top of the inlet blades (in light blue).

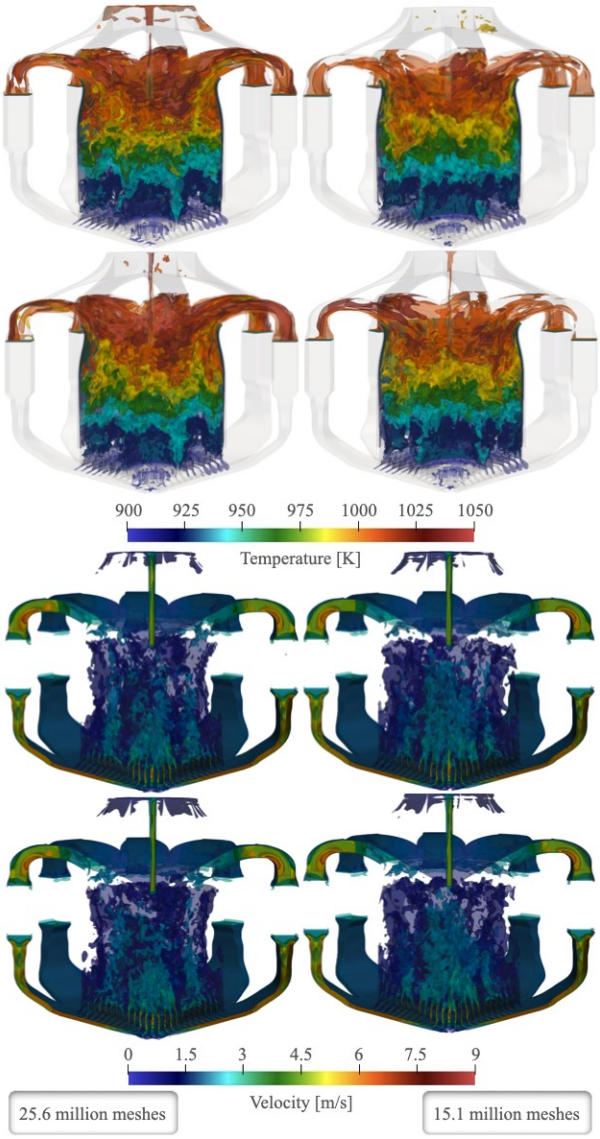

Figure 9: Temperature (top) and velocity (bottom) isovalues for the fine (left) and coarse (right) meshes at different time steps with the proposed optimized design.

3.3. Reactivity comparison

The main driving element for the design optimization performed is the core stability due to thermal fluctuations induced by the turbulence. In this section, a comparison is presented between the EVOL and the proposed designs for both fine and coarse meshes. Figure 10 presents the effective temperature considering an equal weighting between the Doppler (squared flux shape) and the density (flux shape) effects. The standard deviation is computed after the flow stabilization. The temperature fluctuation standard deviation is 1.17 K for the EVOL geometry and 0.18 K for the new geometry. We can see that, as expected, the optimized geometry implies a temperature fluctuation 6.5 times smaller for the fine mesh. Note that a larger value for the preconceptual EVOL geometry is normal since it has not been optimized to reduce the power fluctuation but to homogenize the salt heating in the core. During the EVOL project, only RANS calculations were available for this kind of reactors.

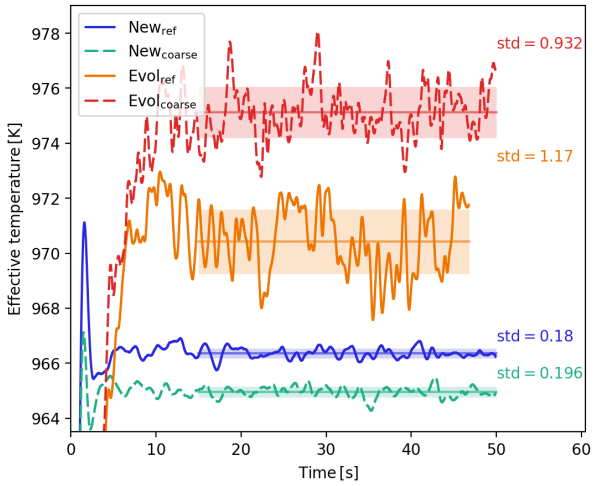

Figure 10: Effective temperature for the EVOL and new proposed designs. The standard deviation is estimated between 15 and 50 seconds.

Note that for a reactor without fertile matter, the Doppler feedback is much smaller than the density feedback. Due to the difference in the feedback distribution (see sec. 2.1.2) the standard deviations of the weighted temperature are 1.13 K for the EVOL geometry and 0.14 K for the new geometry.

In order to estimate the power variation induced by these temperature fluctuations, we can consider an effective fraction of delayed neutrons β_{eff} of 125 pcm [5] as an order of magnitude. With a total feedback of around -8 pcm/K, the reactivity fluctuation $\delta\rho$ is equal to 9.4 pcm for the EVOL geometry and to 1.5 pcm for the new geometry. For a reactivity step ρ, the point kinetic solution gives a power after the prompt jump of $P = P_0 \frac{\beta_{eff}}{\beta_{eff}-\rho}$ [20]. If we consider as a first approximation that the delayed neutron source term is constant and that the prompt kinetics is fast enough to stay at equilibrium, then the power fluctuation

follows a $\frac{\beta_{eff}}{\beta_{eff} \pm \delta\rho}$ law. Finally, for these values of β_{eff} and feedback coefficient, the power variation is around 7.6 % for the EVOL geometry and 1.2 % for the optimized one.

This result can be generalized for different β_{eff} values in figure 11. This phenomenon will be an important point to focus on for future design studies. Increasing the volume of salt in the recirculation loops will decrease the effective fraction of delayed neutrons decaying in the critical region and then increase the power fluctuations accordingly (*i.e.* moving on the left on the curves). The shape of the critical region itself impacts the fluctuation directly as detailed in this article (from the red to the blue curve). Finally, the β_0 is also directly impacted by the fuel composition (larger with ^{238}U and smaller for minor actinides).

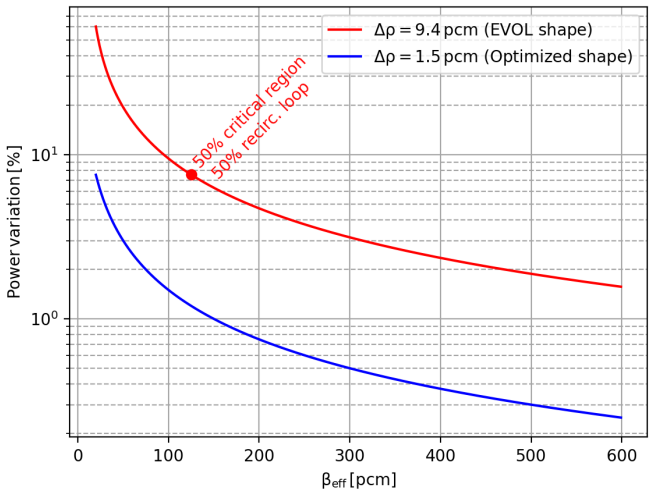

Figure 11: Impact of the reactivity fluctuations on the power variation for different β_{eff} values.

4. Conclusions and perspectives

First DES calculations have been performed to study the power stability of a molten salt reactor with macroscopic turbulence in the critical zone such as the Molten Salt Fast Reactor. The temperature fluctuations induced by the turbulence cannot be neglected since they imply a power fluctuation of around 7.5 % for the EVOL geometry that consists of a core cavity associated to sixteen independent recirculation loops. The temperature fluctuations can be strongly reduced by a dedicated injection system consisting of multiple blades to break the macroscopic eddies that generate the reactivity fluctuations. Thank to this system, the temperature fluctuations are reduced by a factor of 6.5 with the new proposed geometry.

Future studies will focus on the impact of local temperature fluctuations on the walls, and then use a LES instead of a DES model to reduce the modeling uncertainties. Then the mesh requirement will be larger with a y-plus value close to one, leading to a first mesh size of 0.025 mm. According to [13] an ideal near-wall mesh resolution requires an aspect ratio of 1 or a maximum value of 10 for simple shear flows. For this reason, this study will lead to an important increase of the number of meshes in the calculation.

The impact of the design choice (fissile-fertile composition, fraction of salt in the recirculation loop, specific power...) on the fluctuations will also be an interesting point to address in future studies.

References

[1] C. Fiorina, D. Lathouwers, M. Aufiero, A. Cammi, C. Guerrieri, J. L. Kloosterman, L. Luzzi, M. E. Ricotti, Modelling and analysis of the msfr transient behaviour, Annals of Nuclear Energy 64 (2014) 485–498.

[2] M. Aufiero, A. Cammi, O. Geoffroy, M. Losa, L. Luzzi, M. E. Ricotti, H. Rouch, Development of an openfoam model for the molten salt fast reactor transient analysis, Chemical Engineering Science 111 (2014) 390–401.

[3] A. Laureau, P. Rubiolo, D. Heuer, E. Merle-Lucotte, M. Brovchenko, Coupled neutronics and thermal-hydraulics numerical simulations of a molten fast salt reactor (mfsr), in: SNA+ MC 2013-Joint International Conference on Supercomputing in Nuclear Applications+ Monte Carlo, EDP Sciences, 2014, p. 02307.

[4] M. Tiberga, D. Lathouwers, J. L. Kloosterman, A multi-physics solver for liquid-fueled fast systems based on the discontinuous galerkin fem discretization, Progress in Nuclear Energy 127 (2020) 103427.

[5] A. Laureau, D. Heuer, E. Merle-Lucotte, P. Rubiolo, M. Allibert, M. Aufiero, Transient coupled calculations of the Molten Salt Fast Reactor using the Transient Fission Matrix approach, Nuclear Engineering and Design 316 (2017) 112–124.

[6] M. Allibert, M. Aufiero, M. Brovchenko, S. Delpech, V. Ghetta, D. Heuer, A. Laureau, E. Merle-Lucotte, Molten Salt Fast Reactors, in: Handbook of generation IV nuclear reactors, Elsevier, 2016, pp. 157–188.

[7] H. Rouch, O. Geoffroy, P. Rubiolo, A. Laureau, M. Brovchenko, D. Heuer, E. Merle-Lucotte, Preliminary thermal–hydraulic core design of the molten salt fast reactor (msfr), Annals of Nuclear Energy 64 (2014) 449–456.

[8] J.-J. Li, Y.-L. Qian, J.-L. Yin, H. Li, W. Liu, D.-Z. Wang, Large eddy simulation of unsteady flow in gas–liquid separator applied in thorium molten salt reactor, Nuclear Science and Techniques 29 (5) (2018) 1–9.

[9] J. Leppänen, M. Pusa, T. Viitanen, V. Valtavirta, T. Kaltiaisenaho, The Serpent Monte Carlo code: Status, development and applications in 2013, Annals of Nuclear Energy 82 (2015) 142–150.

[10] L. Mathieu, D. Heuer, R. Brissot, C. Garzenne, C. Le Brun, D. Lecarpentier, E. Liatard, J.-M. Loiseaux, O. Meplan, E. Merle-Lucotte, et al., The thorium molten salt reactor: Moving on from the MSBR, Progress in Nuclear Energy 48 (7) (2006) 664–679.

[11] A. Laureau, L. Buiron, B. Fontaine, Towards spatial kinetics in a low void effect sodium fast reactor: core analysis and validation of the TFM neutronic approach, EPJ Nuclear Sciences & Technologies 3 (2017) 17.

[12] H. K. Versteeg, W. Malalasekera, An introduction to computational fluid dynamics: the finite volume method, Pearson education, 2007.

[13] A. Gerasimov, Quick guide to setting up les-type simulations, ANSYS Sweden AB: Goteborg, Sweden (2016).

[14] H. Jasak, A. Jemcov, Z. Tukovic, et al., OpenFOAM: A C++ library for complex physics simulations, in: International workshop on coupled methods in numerical dynamics, Vol. 1000, IUC Dubrovnik Croatia, 2007, pp. 1–20.

[15] G. I. Taylor, Statistical theory of turbulenc, Proceedings of the Royal Society of London. Series A-Mathematical and Physical Sciences 151 (873) (1935) 421–444.

[16] M. S. Gritskevich, A. V. Garbaruk, J. Schütze, F. R. Menter, Development of DDES and IDDES formulations for the k-ω shear stress transport model, Flow, turbulence and combustion 88 (3) (2012) 431–449.

[17] V. Ignatiev, O. Feynberg, A. Merzlyakov, A. Surenkov, A. Zagnitko, V. Afonichkin, A. Bovet, V. Khokhlov, V. Subbotin, R. Fazilov, et al., Progress in development of MOSART concept with Th support, in: Proceedings of ICAPP, Vol. 12394, 2012.

[18] V. Ignatiev, O. Feynberg, A. Zagnitko, A. Merzlyakov, A. Surenkov, A. Panov, V. Subbotin, V. Afonichkin, V. Khokhlov, M. Kormilitsyn, Molten-salt reactors: new possibilities, problems and solutions, Atomic energy 112 (3) (2012) 157–165.

[19] J. Ahrens, B. Geveci, C. Law, Paraview: An end-user tool for large data visualization, The visualization handbook 717 (8) (2005).

[20] J. R. Lamarsh, Introduction to nuclear reactor theory, Addison-Wesley, 1966.